Dissolution of Bioactive Glass S53P4 in Continuous Flows of Tris Buffer and Lactic Acid

Siekkinen, Minna; Engblom, Markus; Karlström, Oskar; Hupa, Leena

Published in:
Biomedical Materials and Devices

DOI:
10.1007/s44174-023-00140-6

Published: 20/11/2023

Document Version
Final published version

Document License
CC BY

Biomedical Materials & Devices
https://doi.org/10.1007/s44174-023-00140-6

ORIGINAL ARTICLE

Dissolution of Bioactive Glass S53P4 in Continuous Flows of Tris Buffer and Lactic Acid

Minna Siekkinen[1] · Markus Engblom[1] · Oskar Karlström[2] · Leena Hupa[1]

Received: 30 August 2023 / Accepted: 10 October 2023

Abstract

In vitro dynamic dissolution of bioactive glass S53P4 particles was studied in a cascade of three reactors. Tris buffer (pH 7.40) and lactic acid (pH 2.00) with flow rates of 0.2 and 0.04 ml/min were fed through the reactors for 24 h. The increased ion concentrations in Tris inflows to the second and third reactors decreased the dissolution of the particles. However, the normalised surface-specific mass loss rate decreased from the first to the third reactor and with decreasing flow rate. No distinct differences were observed in the reaction layers on the particles in the three consecutive reactors. This implied that the ions released in the previous reactors contributed to the reaction layers formed in the following reactors. Highly incongruent dissolution with similar dissolution rates of sodium, calcium, and phosphorus occurred with the two flow rates in lactic acid. Although a thick silica-rich layer formed on the particles, the low pH prevented calcium phosphate layer precipitation. The results imply that S53P4 particles in an implant react at different rates depending on their location but form similar reaction layer morphologies independent of their location in physiological solutions (pH 7.4). On the other hand, S53P4 particles exposed to acidic solutions with a pH < 5 likely dissolve incongruently, leaving a slowly dissolving Si-rich layer. In such an environment, the dissolution rates of Na, Ca, and P are independent of the location of the S53P4 particle in the implant. Thus, the pH and fluid flow are critical factors for the dissolution of S53P4 bioactive glass particles.

Keywords Bioactive glass · In vitro · Biomaterial · Dissolution behaviour · Dynamic · Cascade reactor · Tris-buffer · Lactic acid

Introduction

Bioactive glasses dissolve and react to form surface layers when in contact with aqueous solutions [1]. Since their discovery in the 1960s, bioactive glasses have been studied in many sample forms and various aqueous environments [2]. Today, two bioactive glasses, 45S5 (in wt% $45SiO_2$–$24.5CaO$–$24.5Na_2O$–$6P_2O_5$) [3] and S53P4 (in wt% $53SiO_2$–$20CaO$–$23Na_2O$–$4P_2O_5$) [4] are clinically used chiefly as filler materials for bone cavities [5]. Bioactive glasses' low silica content indicates lower chemical durability than conventional soda–lime–silica glasses [6]. For example, the low durability provides antibacterial properties in vivo due to a rapid exchange of alkali and alkaline earth ions in the glass surface with hydrogen ions in the surrounding solution [7].

The reactions between the bioactive glass and surrounding solution begin with the rapid ion exchange reaction. In this reaction, hydrogen ions (H^+) in the solution form silanol groups (Si–OH) on the glass surface. Phosphate ions (PO_4^{3-}) are also released into the surrounding solution in the initial steps. The decreased H^+ concentration, and thus, the increased pH and hydroxyl ion (OH^-) concentration, lead to the breaking of silicon–oxygen bonds in the glass network. Accordingly, the concentration of dissolved Si species [$Si(OH)_4$] in the solution increases. Then, the insoluble Si–OH at the surface condensates and repolymerises to a silica-rich layer. Ca^{2+} and PO_4^{3-} ions migrate from the bulk glass to the surface and, together with ions from the solutions, precipitate into an amorphous CaO–P_2O_5 layer. After reacting with carbonate, this layer crystallises into

✉ Minna Siekkinen
minna.siekkinen@abo.fi

[1] High-Temperature Processes and Materials, Åbo Akademi University, Henrikinkatu 2, 20500 Turku, Finland

[2] Industrial Engineering and Management, Department of Mechanical and Materials Engineering, University of Turku, Turku, Finland

Published online: 20 November 2023

carbonated hydroxyapatite and provides bonding to the bone apatite. [3, 8]

The reaction steps above are often studied in vitro with simplified solutions mimicking the extracellular body fluid [9, 10]. Conventional in vitro experiments are usually conducted by immersing the bioactive glass sample in static solutions and studying its reactions as functions of time [11]. Circulating the immersion solution has been suggested to mimic the dynamic human body [12]. The environment has been created by replenishing static solutions [13, 14], circulating the solution above a particle bed [15], or introducing a single-pass flow-through setup where an as-prepared solution is continuously fed through the sample [16]. The dynamic in vitro environment is assumed to provide a homogeneous environment, typically seen as more uniform reaction layers on the particle surfaces than in static solutions. Most experiments utilising fluid circulation have been conducted with a fixed flow rate.

The flow rate in bones depends on the diameter and length of the vessels, as well as the differences in the pressure and viscosity of blood [17]. Also, location in the body and the patient's age and health affect the blood flow in the bones [18]. Measuring the exact flow rates inside the bones is challenging, and non-invasive methods for precise measurements are needed. Thus, only estimations based on measuring the flow rate in vessels surrounding the bones are available [19]. One study suggests an intraosseous blood flow rate of 5–20 ml/min per 100 g of bone [20]. In vitro studies in a dynamic environment showed that the reaction behaviour of bioactive glasses markedly varied with the flow rate. During the first 20 min of dynamic dissolution, slower flow rates released ions from the bioactive glass 1–98 (in wt% $53SiO_2$–$22CaO$–$6Na_2O$–$2P_2O_5$–$11K_2O$–$5MgO$–$1B_2O_3$) in a more considerable extent than a faster flow [16]. For bioactive glass S53P4, the pH in the dynamic solution outflow was consistently higher for slower flow rates compared to faster flow rates [21].

The pH highly affects the reactions of bioactive glasses [22]. Most in vitro studies are conducted at a physiological pH of 7.40. However, the local pH around bone infections can be lower, around 5.5–6.7 [23]. Such an environment might build up when bioactive glasses are used to treat, e.g. osteomyelitis in long bones [24–26]. Even though the pH of solutions in contact with bioactive glasses seldom decreases below 5, a reduced local acidic environment may occasionally occur [27]. Additionally, bioactive glasses are used in the oral cavity as dental implants [28], where acidic drinks, e.g. lemon juice and soft drinks, might give a local environment with a pH below 3 [29]. Also, bioactive glass and polylactic acid (PLA) composites have been studied in vitro and in vivo for possible bone replacement [30]. The PLA degrades in body solutions to lactic acid (LA) through hydrolysis [31]. The impact of PLA degradation products on the bioactive glass dissolution in composites is not fully understood. However, initial studies on bioactive glass dissolution in LA suggested that immersed bioactive glass plates gradually turn into silica-rich samples [32]. At the same time, alkali and alkaline ion concentrations increased in static and dynamic solutions [32, 33]. Thus, further studies in LA environments are vital for understanding the glass/solution behaviour in challenging environments and the role of the silica-rich layer as a nucleation site for Ca and P [34].

The dissolution of the bioactive glasses 45S5 and S53P4 in a dynamic environment [35, 36] suggested that the combination of an increased pH, concentrations of released ions, and reaction layers at the glass surface affected but did not wholly hinder further dissolution. Additional in vitro test parameters would increase the utilisation of results in, for example, modelling. Most studies discussing ions dissolving from bioactive glasses focus on the biological and cellular effects. Dissolution products from bioactive glass 45S5 increased osteoblast proliferation, leading to increased bone regeneration [37]. In vitro cell culture studies suggested mineralised human adipose stem cells due to dissolution products from an experimental bioactive glass [38]. The dissolution products from bioactive glass S53P4 promoted fast calcium phosphate (Ca/P) mineralisation in an osteogenic medium [39]. However, estimating the interactions of bioactive glasses with cellular processes in the dynamic environment calls for an enhanced understanding of the impact of fluid flow on ion release.

This study compares the impact of the local fluid environment on the dissolution reactions of bioactive glass S53P4 particles at the physiological pH of 7.40 (Tris buffer) and an acidic solution at pH 2.00 (lactic acid). The solutions were fed through the glass particles in three reactors coupled in a series using two flow rates, 0.04 and 0.2 ml/min. The results provide novel information on the impact of differences in interfacial conditions on the reaction behaviour of bioactive glass particles.

Materials and Methods

Bioactive Glass Particles

Bioactive glass S53P4 was melted in-house from quartz sand (SiO_2) and analytical grade reagents [$CaCO_3$, Na_2CO_3, and $CaHPO_4{\cdot}2(H_2O)$] at 1360 °C in an electric furnace for 3 h. The melt was cast to a bar in a graphite mould, annealed for 1 h at 520 °C and then cooled to room temperature overnight. The bar was crushed, remelted, and annealed for homogeneity. Then, the glass was crushed with a ring and puck mill. The glass particles were sieved to a size range of 300–500 µm. The particles were cleaned with acetone in an ultrasound bath to remove the powder attached to the

surfaces. Fine powder dissolving rapidly or transported by the fluid flow through the reactor filter would challenge the accuracy and interpretation of the dissolution mechanisms.

The crushed and cleaned particles were stored in a plastic bag in a desiccator until further use. The particle size distribution (Malvern Panalytical Mastersized 3000) and an SEM image (scanning electron microscope; Leo Gemini, Carl Zeiss) of the crushed and cleaned particles are shown in Fig. 1. The elongated particles passed through the 500 µm sieve and increased the size distribution beyond the range, as seen by the curve and SEM image. The measured surface area moment mean (D[2,3]) was 493 µm, and the volume moment mean (D[3,4]) was 526 µm. The size fraction's specific surface area (SSA) was 4.686 m^2/kg.

In Vitro Solutions

This work studied the ion release from S53P4 into Tris buffer (Tris) and lactic acid (LA). Tris buffer was used as a reference for dissolution into a simplified medium. For 1 l of Tris buffer, 6.057 g of tris(hydroxymethyl)aminomethane (Fisher Chemical) was dissolved in 900 ml of purified water (ELGA Veolia). The temperature of the solution mixture was increased to 37 °C in a water bath before adjusting the pH with 1 M HCl to 7.40. LA enabled estimating the impact of an acidic dynamic environment on bioactive glass dissolution. 0.4 M lactic acid was prepared by adding 35 ml of 85% DL-lactic acid (Sigma) to 965 ml of purified water to give a solution pH of 2.00.

Dissolution Study

Dissolution Setup

The setups for the continuous flow-through reactors have been described elsewhere [16, 35]. One, two, or three polypropylene reactors were coupled in a series to a cascade reactor to allow the analysis of the outflows from each reactor combination and particles in each reactor. 210 ± 5 mg of S53P4 particles were placed in each reactor, and the solution was fed through them with 0.04 or 0.2 ml/min using a peristaltic pump (Ismatec IPC High Precision Multichannel Pump). The lower flow rate was chosen to fit into the suggested flow rate of 5–20 ml/min per 100 g of bone [20], whilst the faster flow rate has been used in our previous studies. The pump was connected to the solutions and reactors with thin thermoplastic tubes (Tygon®). The solutions and reactors were kept in a 37 °C water bath during the dissolution. For the flow rate of 0.04 ml/min, the solution outflow was collected for 1 h (2.4 ml) every hour for up to 8 h and then at hour 24. For the solution flow rate of 0.2 ml/min, the solution outflow was collected for 20 min (4 ml), every 20 min for the first hour, then every other hour for up to 8 h, and finally, at hour 24. The measured values are given for the endpoint of each solution collection. Parallel static experiments were also conducted as a control using 210 ± 5 mg of S53P4 particles immersed in 30 ml Tris and LA in a 100 rpm shaking incubator (Stuart Orbital Incubator SI500) at 37 °C. At 24 h, the reactions were stopped by washing with ethanol, followed by drying the particles overnight at 40 °C. Each experiment was done in triplicates.

Solution pH

The pH meter (VWR, pHenomenal pH 1100 L) was calibrated with standardised buffer solutions (4.01 and 7.00, VWR). The pH measurements were conducted directly in a water bath directly after the solution collection. Each reported value is an average of three parallel measurements. The pH of the static solutions was measured from the supernatants as close to the particles as possible without the electrode touching the particle beds at 2, 4, 6, 8, and 24 h. The pH of the reference solutions was measured before and after each experiment.

Ion Release

The ion concentrations were measured with inductively coupled plasma-optical emission spectrometry (ICP-OES, Optima 5300 DV; Perkin Elmer). Three parallel

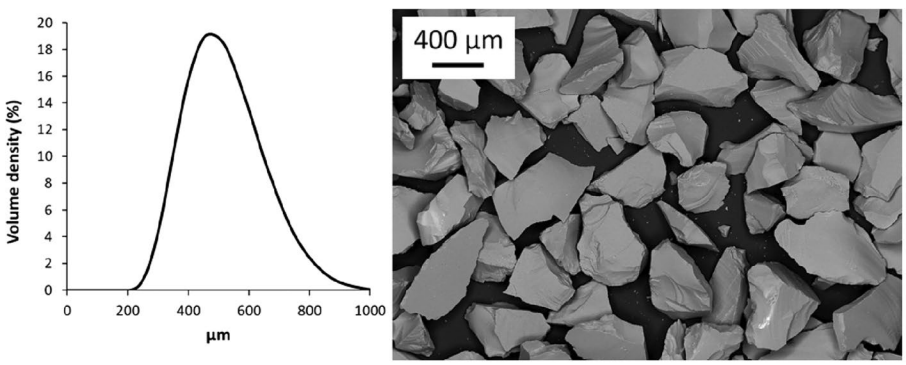

Fig. 1 Size distribution of S53P4 particles crushed and sieved to 300–500 µm size range (left) and SEM image of crushed and cleaned particles (right)

samples from each time point were analysed 3–5 times. The ICP-OES was calibrated with 1, 5, and 20 ppm of Si, Ca, Na, and P (Spectrascan) between every 60 samples. The reported results are background corrected accordingly. The limit of quantification and wavelengths were Si = 0.04 ppm; 251.622 nm, Ca = 0.003 ppm; 317.933 nm, Na = 0.2 ppm; 589.592 nm, and P = 0.03 ppm; 213.617 nm.

Normalised Surface-Specific Mass Loss

The measured ion concentrations were converted into normalised surface-specific mass loss rate according to Eq. (1) [16]:

$$\mathrm{NR}_i = \frac{C_i}{f_i\left(\frac{\mathrm{SA}}{F}\right)}, \tag{1}$$

where C_i is the concentration of element i (mg/l), f_i is the mass fraction of element i in the glass, SA is the initial total surface area of the glass particles (m^2), and F is the flow rate of the solution (m^3/s). Equation (1) gives the normalised surface-specific mass loss rate (NR_i) for element i at a desired time point (g m^{-2} s^{-1}). The initial total surface area was calculated from the analysed specific surface area (4.686 m^2/kg) and the initial mass of bioactive glass particles. NR_i was calculated for each element for the bioactive glass dissolution to the two solutions at the two flow rates.

Reaction Layers

After the dissolution, the glass particles were cast in epoxy resin for analysis with a scanning electron microscope coupled to an energy-dispersive X-ray (EDX; Thermo Scientific UltraDry, Thermo Scientific). The embed particles were ground and polished with ethanol and abrasive paper to reveal the cross-sections.

Results

Solution pH

Figure 2 shows the pH of Tris and LA in the dynamic and static experiments as functions of time. The results for the experiments using 0.2 ml/min Tris and static Tris have been reported earlier [36, 40]. The pH graphs do not include deviations of the parallel measurements as most were below ± 0.05 pH units, with a maximum deviation of ± 0.12. The pH increased during the first hour and then gradually decreased towards the values before dissolution.

For both solutions, the highest pH was measured after three reactors at 1 h for the flow rate of 0.04 ml/min. The pH was consistently higher in the slower flow than in the faster one. In each experiment, the pH of Tris was within the solution's buffering capacity range. In contrast, the pH of the static solutions increased slowly during the immersion. At 24 h in Tris, the pH of the static solution was the same as after one reactor in the cascade reactors for both

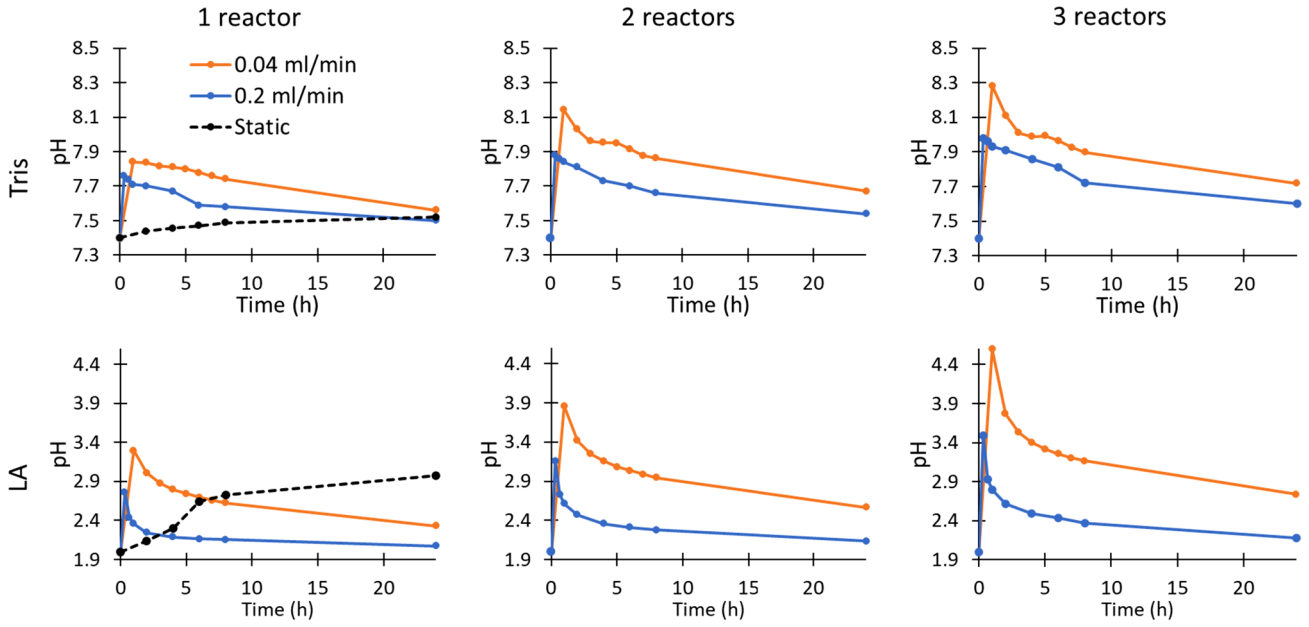

Fig. 2 Change of pH in the outflow of dynamic and static 0.05 M Tris (pH 7.4) and 0.4 M lactic acid (pH 2.00) with an increasing number of reactors horizontally. Static and 0.2 ml/min Tris are from results reported elsewhere [36, 40]

flow rates. In contrast, the pH of the static LA corresponded to the value after three reactors for the 0.04 ml/min flow rate at 24 h.

Ion Release

Tables 1 (Tris) and 2 (LA) show the average ion concentrations (mg/l) in the outflows measured with ICP-OES. Also, results in Tris using the flow rate of 0.2 ml/min are included [36]. The ion concentrations at 24 h static experiments in Tris [40] and LA are marked in the table using the symbol 24S. The highest deviations (± 13 mg/l Na in Tris, and ± 200 mg/l Ca in LA) were measured for the slowest flow rate and at the first measurement points. The deviations are omitted from the table for clarity. The significant difference in the solution volume fed through the reactors using the two flow rates explains the concentration differences between the two flow rates at each time point. The total solution volumes consumed during the 24 h were 57.6 and 288 ml for the flow rates of 0.04 and 0.2 ml/min, respectively. Although the concentrations of released ions into Tris increased with the number of reactors, the relative increases in the second and third reactors were markedly less than in the first reactor. In contrast, the dissolved ion concentrations in LA increased after each reactor equally.

Reaction Layers

SEM–EDXA of particles reacted for 24 h in 0.2 and 0.04 ml/min Tris are shown in Fig. 3. Si concentration increased in all reactors from the bulk glass towards the glass surface. Increased Ca and P concentrations at the outermost surfaces suggested calcium phosphate (Ca/P) precipitation. However, no pure Ca/P was analysed on particles from any reactor, as silicon was also present in the outer layer. The reaction layers developed similarly on the particles in both flow rates. However, the precipitated Ca/P layer was slightly thicker at the 0.2 ml/min flow rate. Also, the silica-rich layer was thicker on the third reactor particles in the faster flow.

Figure 4 shows SEM micrographs and line analyses of cross-sections of particles after 24 h of continuous LA flow. Contrary to Tris, an almost pure silica-rich layer had formed on the particle surfaces. No distinct difference was observed between the thickness of the layers when comparing the reactor number or flow rate.

Figure 5 shows SEM images of particles from experiments in static and dynamic 0.04 ml/min LA for 24 h. A more even silica-rich layer had formed on particles in the dynamic than in the static system. The formed layer was also thicker on the particles in the dynamic fluid flow.

Table 1 Measured ion concentrations (mg/l) in 0.05 M Tris outflows after 1, 2, or 3 reactors for 0.2 ml/min [36] and 0.04 ml/min, n/a = < LOQ

	Si						Ca					
	0.2 ml/min			0.04 ml/min			0.2 ml/min			0.04 ml/min		
h	1	2	3	1	2	3	1	2	3	1	2	3
1	68	80	95	83	106	126	92	123	155	162	204	223
2	70	78	82	82	91	95	83	108	131	128	178	189
4	67	73	78	78	81	83	68	93	118	114	144	151
6	63	69	74	75	77	80	57	79	107	106	130	144
8	61	66	69	70	74	76	47	64	86	89	116	128
24	53	59	62	55	65	70	30	39	51	43	71	84
24S	12						19					
	Na						P					
	0.2 ml/min			0.04 ml/min			0.2 ml/min			0.04 ml/min		
h	1	2	3	1	2	3	1	2	3	1	2	3
1	119	165	205	212	305	365	8.8	8.4	11	10	4.8	2.8
2	109	156	192	176	246	277	7.7	4.5	3.8	4.7	5.5	5.2
4	89	133	178	167	211	232	6.9	4.8	2.8	1.2	n/a	0.4
6	73	110	164	154	203	219	6.0	4.9	2.8	1.6	0.6	0.6
8	59	88	125	130	177	195	5.3	4.8	3.9	2.1	0.9	0.8
24	37	48	65	55	100	123	4.1	4.6	5.4	3.6	3.1	2.0
24S	31						0.5					

24S gives the concentration after 24 h of static dissolution in Tris [40]

Table 2 Measured ion concentrations (mg/l) in the outflow of 0.4 M lactic acid after 1, 2, or 3 reactors for 0.2 ml/min and 0.04 ml/min

	Si						Ca					
	0.2 ml/min			0.04 ml/min			0.2 ml/min			0.04 ml/min		
h	1	2	3	1	2	3	1	2	3	1	2	3
1	2.2	4.4	6.4	15.8	31.7	48.6	211	409	582	1489	2640	3627
2	2.1	4.3	5.8	10.4	19.9	30.6	138	283	399	863	1659	2475
4	2.2	4.3	6.2	9.9	18.4	26.8	103	206	296	585	1131	1673
6	2.5	4.6	6.5	10.2	18.7	26.5	86	169	248	469	909	1314
8	2.8	4.8	6.9	10.8	19.9	26.7	71	143	209	402	809	1142
24	3.8	6.8	9.8	16.0	25.4	34.1	32	64	91	171	330	512
24S	3.2						154					
	Na						P					
	0.2 ml/min			0.04 ml/min			0.2 ml/min			0.04 ml/min		
h	1	2	3	1	2	3	1	2	3	1	2	3
1	233	456	654	1625	2869	3963	25	49	71	187	319	449
2	152	316	446	932	1760	2614	16	35	48	109	226	338
4	112	231	334	630	1201	1771	12	25	37	74	142	210
6	94	190	278	504	981	1439	10	21	31	59	114	168
8	79	162	234	434	857	1226	9	18	26	51	102	144
24	35	70	104	202	363	552	4	8	12	22	42	65
24S	269						11					

24S gives the concentrations after 24 h of static dissolution in LA

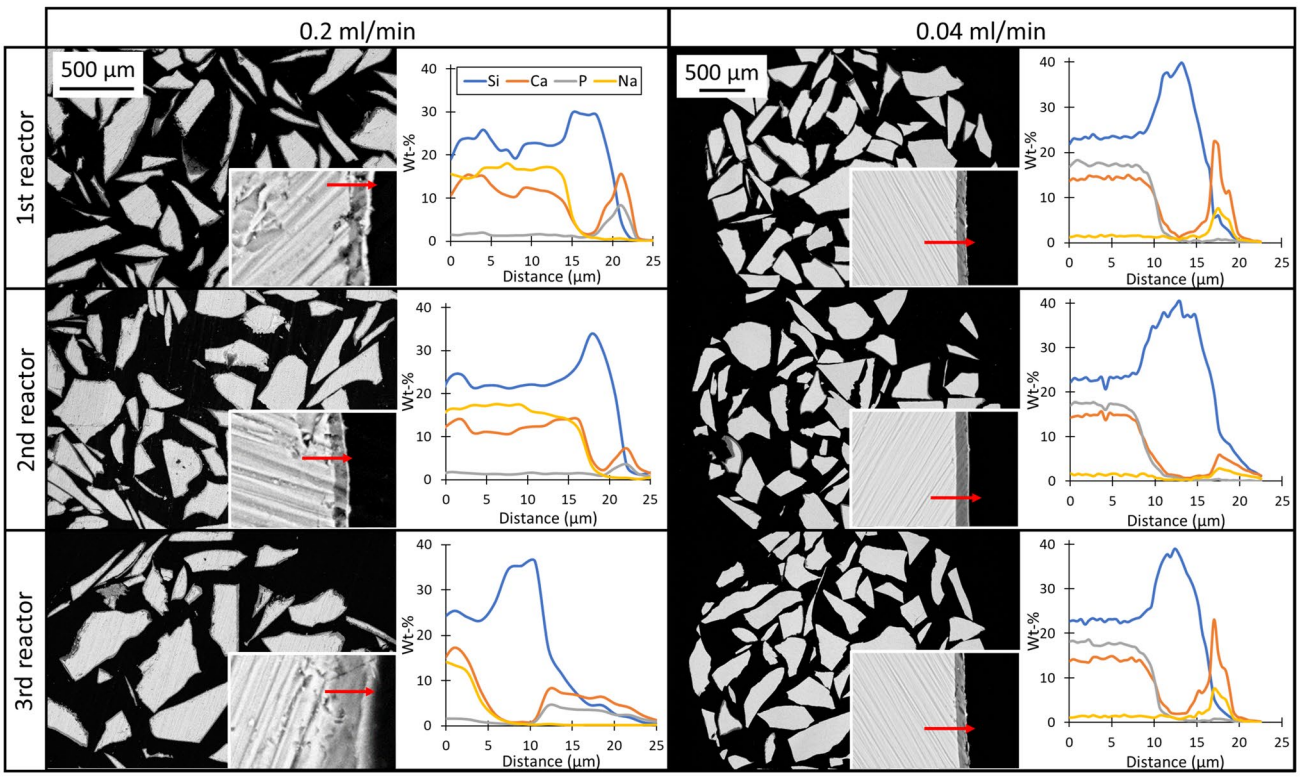

Fig. 3 SEM–EDXA of S53P4 particles in the three reactors in experiments conducted with 0.2 and 0.04 ml/min Tris for 24 h. Each arrow in the magnified figure corresponds to 25 µm

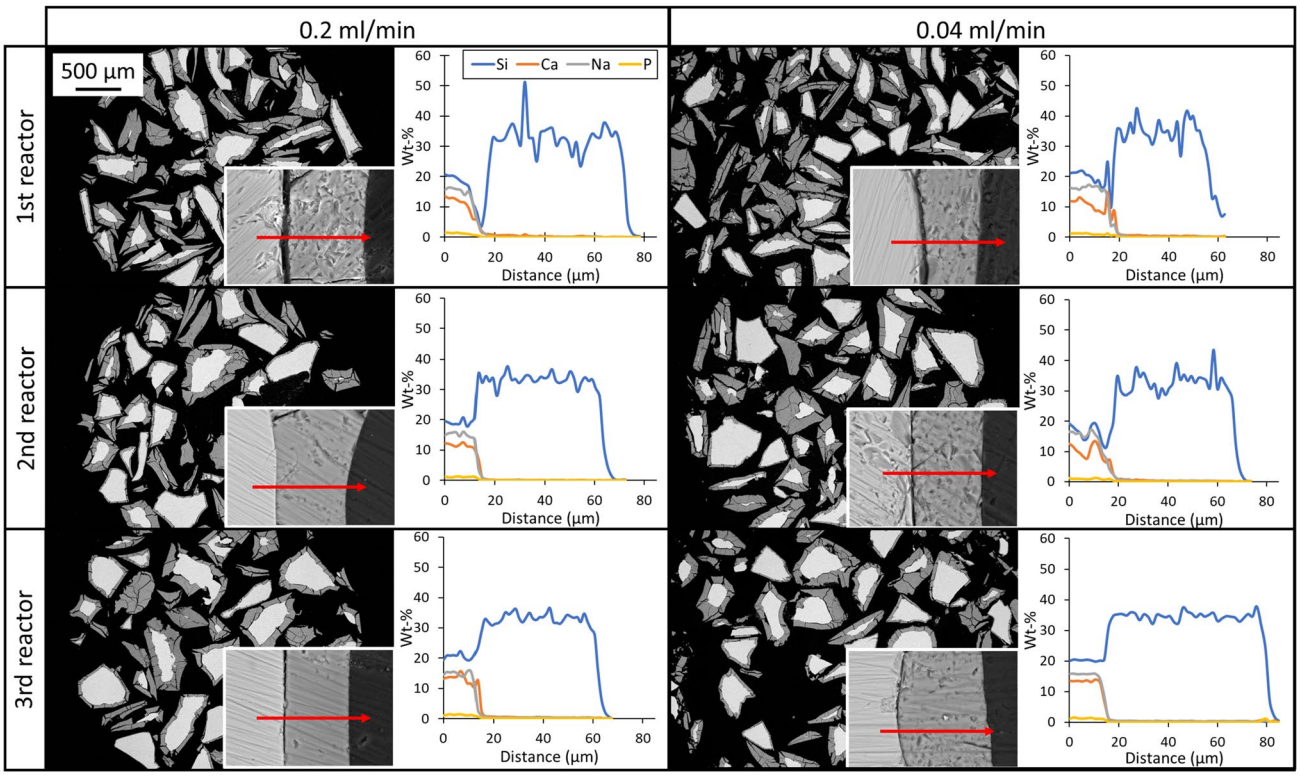

Fig. 4 SEM–EDXA of S53P4 particles in the three reactors after dynamic lactic acid exposure for 24 h. Each arrow in the magnified figure corresponds to 80 µm

Discussion

This work studied the impact of ions released from bioactive glass S53P4 on the dissolution trends of neighbouring glass particles in dynamic solutions of Tris (pH 7.40) and lactic acid (pH 2.00) using two flow rates of 0.04 and 0.2 ml/min. Static immersions served as references. The dynamic dissolution studies were performed in a cascade system of three reactors to analyse changes in the solution composition (ICP-OES) and particle surface composition (SEM–EDXA) with progressive dissolution during 24 h. In contrast to conventional static immersion studies where pH and ion concentrations increase gradually [41, 42], these values first increased rapidly, decreasing then towards the values in the reference solutions (Fig. 2; Table 1).

The ion dissolution into Tris gradually decreased with time after the initial dissolution peaks of all ions around one hour. Despite the significant differences in the solution volume fed through the samples using the two flow rates, the concentration of silicon species released into Tris at 24 h was on the same level, around 55 mg/l in the first reactor (Table 1). Similarly, the Si release was much less, 10 mg/l or lower, from the second reactor for the two flow rates, whilst still less dissolved from the third reactor particles. The lower Tris flow rate led to clearly higher calcium ion release throughout the 24 h dissolution. Sodium ion concentration after the first reactor was higher for the lower flow rate. Calcium and sodium ion concentrations released from the second and third reactor particles were significantly lower than from the first reactor. The phosphate concentrations suggested that all phosphate released from the particles in the first reactor had formed calcium phosphate in the two following reactors. Especially the sodium concentration was relatively high after the third reactor. This implies that toxic effects due to locally high ion concentrations must be considered for bioactive glasses containing elements critical for tissue healing and regeneration at elevated concentrations.

SEM–EDX results suggested some calcium phosphate on the particles' outer surface (Fig. 3). The thicknesses of the reaction layers were almost similar for both flow rates of Tris. However, the precipitated Ca/P layer was slightly thicker in the faster flow. This suggests that Ca/P precipitated faster due to the increased Ca and P concentrations in the faster Tris flow. Silica-rich and Ca/P layers were identified on the particles, although the ion dissolution decreased after the first reactor (Table 1). Likely, the ions dissolved from the first reactor particles in Tris contributed to the layer growth in the consecutive reactors. Thus, the increasing ion concentrations retarded the glass dissolution but did not significantly affect the reaction layer morphology of the glass

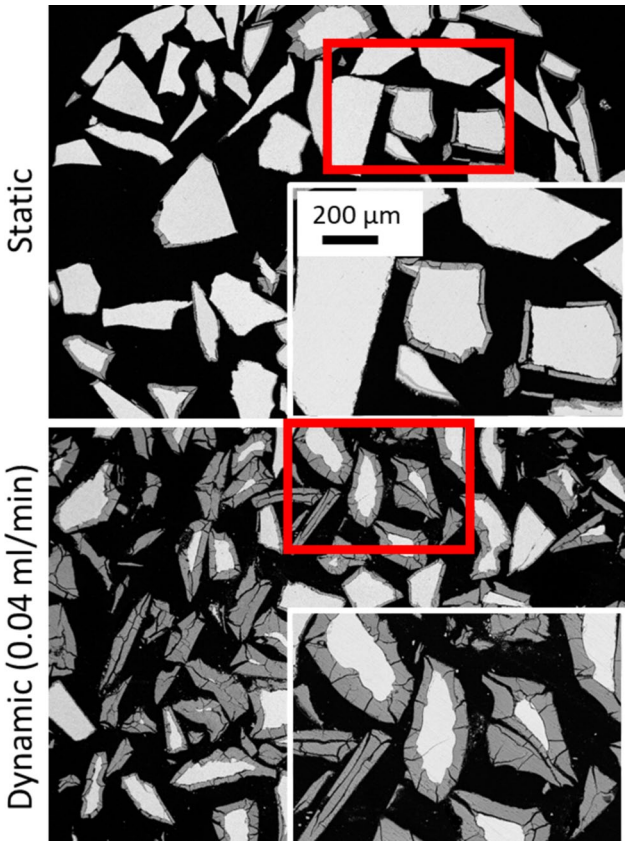

Fig. 5 S53P4 particles after 24 h in static LA (above) and 0.04 ml/min LA in the 1st reactor (below)

particles in Tris. The particle surface composition implies that the primary silica-rich layer on the first reactor particles, i.e. particles representing exterior particles in a bed, was due to ion exchange. At the same time, dissolved species recondensed in the subsequent reactors representing interior particle behaviour as soon as suitable nucleation sites had formed on them. Compared to static conditions, the ion release concentrations suggested similar trends, i.e. high release of sodium ions, some silicon species released, and precipitation of Ca/P. The incongruent and particle unspecific dissolution in LA led to similar silica-rich layers on all glass particles in the three reactors (Fig. 4).

Interestingly, the ion release into LA showed different trends. First, the release of silicon species was much less than in Tris. The relative ion release from each reactor stayed on similar levels, independent of the concentration in the inflow. The dissolution of Si was around 9–16 mg/l for the slower flow rate, 0.04 ml/min, at 24 h. Less silicon dissolved into each reactor using the faster flow rate, around 3–4 mg/l. In contrast, calcium, sodium, and phosphorus were readily released from the glass particles. Similar results due to accelerated ion exchange and alkali hydrolysis have been reported for alkali aluminoborosilicate glasses in static HCl (pH 2.00) [43]. The SEM images showed thick silica-rich surface layers without signs of calcium phosphate precipitation (Fig. 4). Fast dissolution kinetics in an acidic static environment has been reported to lead to faster polymerisation of the silica-rich layer [44]. In this work, the pH after the reactors did not significantly increase due to the continuous feed of as-prepared LA. Further, no calcium phosphate precipitated (Figs. 4, 5) because calcium compounds dissolve in acidic solutions [45]. The solution pH did not in any experiment increase above 5, i.e. levels at which amorphous calcium phosphate precipitates [46]. Calcium and phosphate ions released were likely effectively chelated by LA [47]. Whether this means that lactic acid produced in the degradation of polylactide-based biopolymers prevents hydroxyapatite precipitation in a PLA-bioactive glass composite needs further study.

The pH of Tris stayed within the stability range of Ca/P precipitation and the silica-rich layer provided suitable nucleation sites during the dynamic and static experiments (Figs. 2, 3). On the other hand, increased dissolution of amorphous silica occurs in solutions with a pH above 8 [48] and Si dissolution from a two-component glass was promoted in alkaline solutions with a pH well above 9 [49], consequently leading to a decreased silica-rich layer for Ca/P-precipitation. In this work, the pH of Tris outflows was below 8.28. However, the pH inside the particle beds might have been higher locally than the measured pH of the outflow solutions [15]. Thus, the changes in Si species concentrations after the first reactor (Table 1) indicate that the local pH stayed below the level leading to increased Si dissolution (Tris). Thus, the continuous solution feeds prevented high local pH and promoted dissolution. Similarly, a large reactor study in vitro with 3 µm/s SBF flow over a bioactive glass 13–93 implant concluded that the dynamic environment allowed the pH to stay below levels that would impact the reaction behaviour [50].

Apart from our previous reports implementing a cascade reactor system [35, 36], studies on the impact of bioactive glass ion dissolution products on the reactions of nearby glass particles are sparse. Further, to the authors' knowledge, studies of the effects of dissolution products on the reactions of neighbouring bioactive glass particles in LA are limited [32, 33]. Alkali and alkaline ion release in these studies was higher than in physiological pH. Furthermore, bioactive glass 45S5 neutralised replenished LA (pH 4.00) when incorporated in a resin composite [51].

Figure 6 shows the share (wt%) of the dissolved elements (silicon, calcium, sodium, and phosphorus) in dynamic Tris and LA. The dissolution was calculated from the ion concentration differences between outflows and inflows (Tables 1, 2), the volume of solution flowing through the setup, and the total mass of the elements in the unreacted glass. In 0.04 ml/min Tris, the dissolution decreased in the consecutive

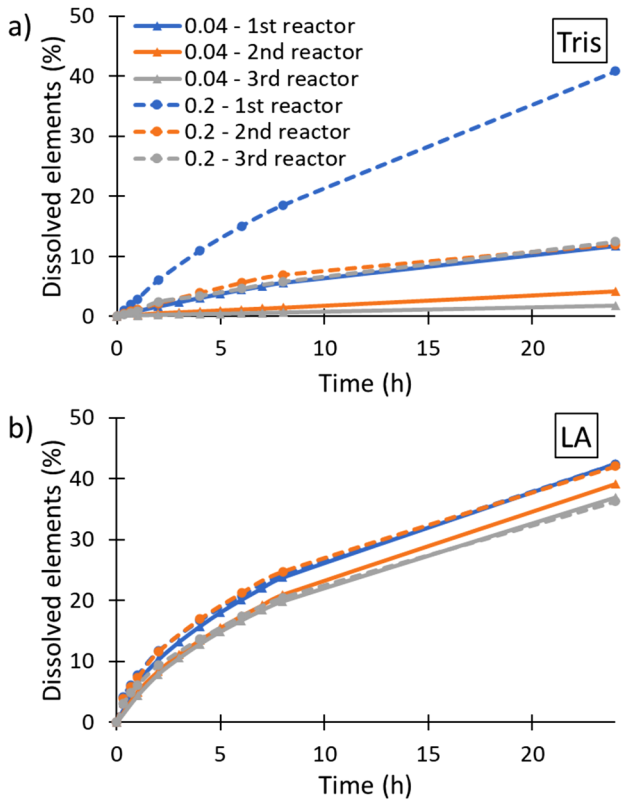

Fig. 6 Cumulative dissolution of Si, Ca, Na, and P to dynamic Tris (**a**) and LA (**b**) for 24 h of continuous flow-through with 0.04 and 0.2 ml/min solution flow

reactors from 12% in the first reactor, to 4 and 1.8% in the second and third reactors. In contrast, the total dissolution decreased from 41% (first reactor) to 12% (second and third reactors) for the faster flow rate. The decreasing dissolution suggests that the dissolved ions in the solution flowing into the second and third reactors decreased the dissolution. At the same time, the reaction layer morphologies were almost similar (Fig. 3). Likely, the dissolved ions from the first and second reactor particles contributed to the layer formation by recondensation and precipitation in the consecutive reactors. On the other hand, no similar decrease was measured in the dissolution in the consecutive reactors in LA at 24 h. The dissolution consisting mainly of Ca, Na, and P varied between 36 and 42% in both flow rates. In the static conditions, the dissolution was 1.5% in Tris and 10% in LA at 24 h. The differences in the dissolution degrees and reaction layer morphologies were assumed to depend on lower concentration gradients in the interfacial solution inside the particle bed in dynamic conditions compared to the static systems. The location of the S53P4 particles in the particle beds, the solution pH, and the flow rate thus affected the dissolution rate. Accordingly, a thorough understanding of the fluid flow rate around and within an implant is crucial for tailoring a bioactive glass-based implantable device.

Figure 7 shows the calculated normalised surface-specific mass loss rate (NR_i) for the glass particles in each reactor as a function of time for experiments conducted in Tris for the two flow rates. Although the ion concentrations measured were higher for the slower flow rate, a higher share of glass

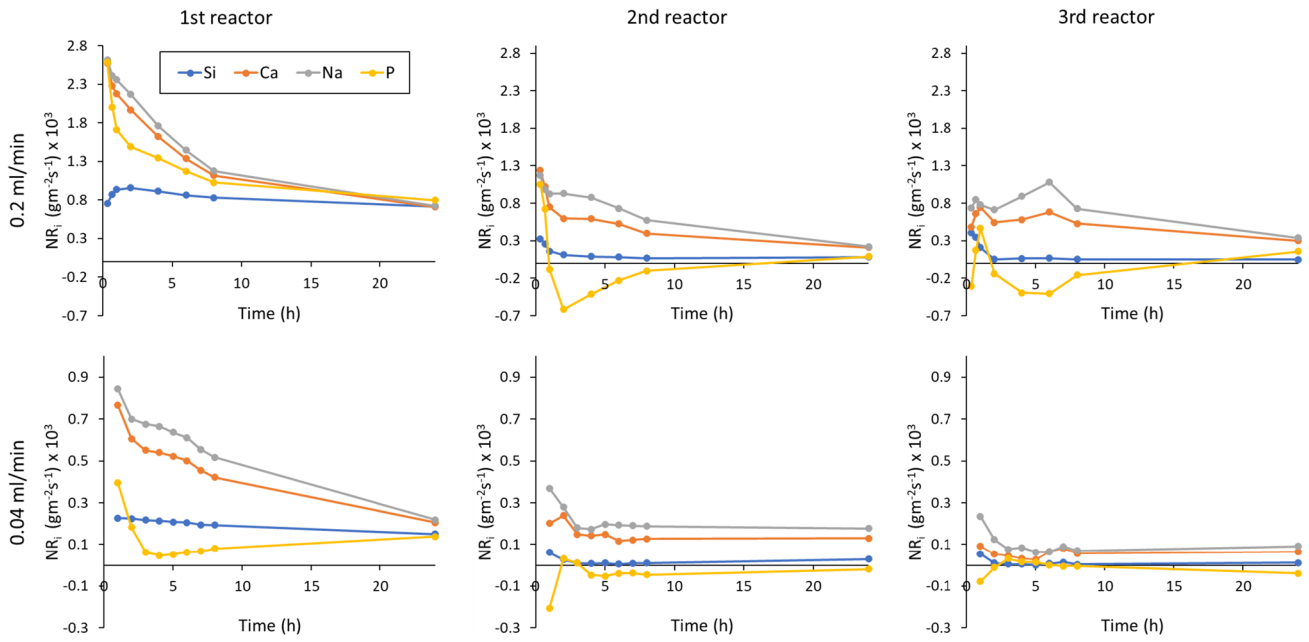

Fig. 7 Normalised surface-specific mass loss rate for S53P4 particles in experiments with 0.2 and 0.04 ml/min Tris for the three consecutive reactors

was dissolved in the Tris buffer fed with a higher flow rate after 24 h, explained by the larger total solution volume fed through the reactors. Accordingly, the normalised surface-specific mass loss rate was higher for the higher flow rate. The normalised dissolution trends also imply decreased rates with the increasing number of reactors. The higher flow rate gave a higher NR_i for all elements. The elements initially leached at different rates (incongruent dissolution) with higher rates for Ca, Na, and P than Si. The dissolution in the first reactor with a flow rate of 0.2 ml/min was congruent at 24 h. In the two other reactors, the initially incongruent dissolution also approached congruent dissolution at longer times. The differences between Ca and Na rates were assumed to depend on the precipitation of Ca/P based on the P dissolution trends. The ion release trends to the lower Tris flow rate showed similar trends but slower normalised dissolution as the higher flow rate. However, the lower dissolution is seen as a much lower normalised dissolution. Ca/P precipitation was assumed based on the line analyses of the reaction layers (Fig. 3). Negative P-values in the second and third reactors in Fig. 7 also indicate Ca/P precipitation. The dissolution rate of P was markedly less in the consecutive reactors and the lower flow rate. In vivo, Ca/P precipitation is likely more rapid due to the higher ion concentrations in the physiological solution.

Calculated NR_{Si} in LA are presented in Fig. 8. In contrast to Tris, the surface-specific mass loss rates of Ca, Na, and P were similar throughout the experiments. Thus, the particles dissolved similarly in all three reactors at both flow rates. Correspondingly, the surface-specific Si mass loss rate was much lower. NR_{Si} was slightly higher in the first reactor for both flow rates. As the silica-rich layer thickness was almost equal on particles in each reactor, the slightly higher release rate in the first reactor might indicate a recondensation of silicon species in the second and third reactor particles.

Studies in a dynamic environment are limited, and most have used a flow rate of 0.2 ml/min [35, 36, 52–54]. A slower fluid flow rate has been suggested to increase the ion exchange [21, 55]. This study showed higher ion concentrations in slower flows of Tris and LA (Tables 1, 2). The lower flow rate (0.04 ml/min per 0.210 g glass) was still on the higher end of the estimated blood flow in bones [20]. Thus, lower rates are recommended for future studies to understand the impact of ion release from bioactive glasses. NR_i of Ca, Na, and P were considerably higher in LA than in Tris. Interestingly, the NR_i values were similar regardless of the reactor and flow rate. This aligns with the increased ion release of Ca and P from bioactive glass 45S5 in a 0.56 ml/min dynamic acetic acid sodium acetate buffer (pH 4) compared to the Tris-buffered simulated body fluid [56].

The three-step cascade reactor in this study can be compared with a bed of implanted bioactive glass particles. The first reactor in the cascade is proposed to mimic the outer part of the implanted particles in first contact with the solution. The solution with the dissolved ions then flows further in the implanted particle bed, mimicked in vitro by

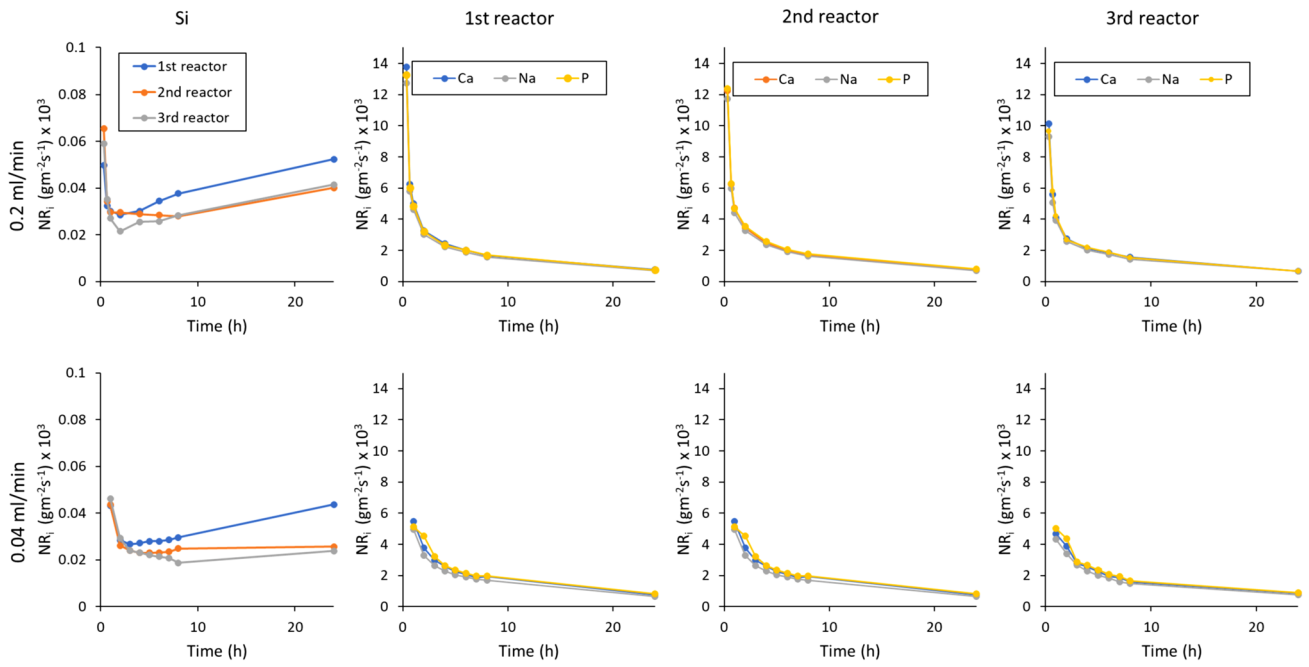

Fig. 8 Normalised surface-specific mass loss rate for S53P4 particles in experiments with 0.2 and 0.04 ml/min LA for the three consecutive reactors

the second and third reactors in the cascade. The results in this study, combined with previously reported results [35, 36], suggested that dissolved ions decreased the surface-specific mass loss rate after the first reactor at pH 7.4. In contrast, a similar decrease was not noticed at the acidic pH. This implies that the implanted particles would dissolve incongruently and similarly in an acidic solution. Thus, the dissolved ions would not affect the ion release from the neighbouring particles or condense on these if the pH stays well below levels where Ca/P precipitation takes place. For a PLA composite implant, gradual polymer degradation would lead to an incongruent dissolution of bioactive glass particles if the local pH was less than around pH 5, independent of the fluid flow rate or the glass particle location in the implant. In contrast, implanted bioactive glass particles would dissolve at different rates depending on their location in physiological solutions (around pH 7.4).

The dissolution rate of a bioactive glass depends not only on its composition but also, to a great extent, on the local pH environment. Temperature also affects the dissolution kinetics and mechanism [16] but has a minor impact in the narrow body temperature range. Further, the porosity of the implant and the fluid flow rate around and through the implant affect the dissolution rate and mechanism. Interestingly, the reaction layers in different locations of a porous S53P4 scaffold implanted in the rabbit femur were similar [57].

The results of this study provided some insights into the impact of the pH environment on the reactions in different implant parts for designing devices based on bioactive glass to various fluid flow conditions. Longer runs in the continuous flow conditions are needed to better understand the long-term fate of the glass and how the findings correlate with the in vivo behaviour.

Conclusion

Dissolution behaviour and reaction layers were studied for bioactive glass S53P4 particles in a dynamic cascade reactor system in physiological (Tris buffer solution, pH 7.4) and acidic (lactic acid, pH 2.00) conditions. In Tris, the ion concentration increased in the solution inflow to the second and third reactors, leading to decreased ion release from the particles in these reactors. In contrast, the dissolution was less affected by the changes in the ion concentrations in the acidic solution. The cascade reactor enabled following the impact of ions dissolved from the glass particles on the reaction behaviour of nearby particles. Despite the decreasing ion release in Tris, the reaction layer thicknesses were equal on the particles in the three reactors at 24 h. Thus, the dissolved ions readily recondense on particles, decreasing the dissolution at physiological pH. However, the dissolved ions only slightly affected Si release or reaction layer thicknesses in lactic acid. The glass particles dissolved incongruently and at almost the same rate, independent of their location in the lactic acid flow. The slower flow of the Tris (0.04 ml/min) gave higher ion concentrations in the outflow than the faster rate (0.2 ml/min). The normalised surface-specific mass loss rate decreased with the flow rate. Correlating the results with an implanted bioactive glass particle bed suggested that particles inside the bed react slower than exterior particles in the physiological pH range. In contrast, inside a system where pH might decrease to around 2, e.g. due to a degrading biopolymer composite, the bioactive glass particles would dissolve incongruently and similarly throughout the implant. How an acidic degradation of polylactic acid in a bioactive glass composite would locally affect the bioactive glass reactions in the physiological pH range is unclear and needs further study.

Acknowledgements Financial support by Victoriastiftelsen (Project 20230362) is acknowledged (Siekkinen). Luis Bezerra and Linus Silvander are acknowledged for their technical help with ICP-OES measurements and SEM–EDX analysis.

Funding Open access funding provided by Åbo Akademi University.

Data Availability Data will be made available on reasonable request.

Declarations

Conflict of interest There are no conflicts of interest.

References

1. L.L. Hench, Bioceramics: from concept to clinic. J. Am. Ceram. Soc. **74**, 1487–1510 (1991). https://doi.org/10.1111/j.1151-2916.1991.tb07132.x
2. L.L. Hench, The story of Bioglass®. J. Mater. Sci. Mater. Med. **17**, 967–978 (2006). https://doi.org/10.1007/s10856-006-0432-z
3. L.L. Hench, Bioceramics. J. Am. Ceram. Soc. **81**, 1705–1728 (1998)
4. Ö.H. Andersson, I. Kangasniemi, Calcium phosphate formation at the surface of bioactive glass in vitro. J. Biomed. Mater. Res. **25**, 1019–1030 (1991). https://doi.org/10.1002/jbm.820250808
5. E. Fiume, J. Barberi, E. Verné, F. Baino, Bioactive glasses: from parent 45S5 composition to scaffold-assisted tissue-healing therapies. J. Funct. Biomater. **9**, 24 (2018). https://doi.org/10.3390/jfb9010024

6. L.L. Hench, D.E. Clark, Physical chemistry of glass surfaces. J. Non-Cryst. Solids **28**, 83–105 (1978). https://doi.org/10.1016/0022-3093(78)90077-7
7. E. Munukka, O. Leppäranta, M. Korkeamäki, M. Vaahtio, T. Peltola, D. Zhang, L. Hupa, H. Ylänen, J. Salonen, M. Viljanen, E. Eerola, Bactericidal effects of bioactive glasses on clinically important aerobic bacteria. J. Mater. Sci. Mater. Med. **19**, 27–32 (2008). https://doi.org/10.1007/s10856-007-3143-1
8. J.R. Jones, Review of bioactive glass: from Hench to hybrids. Acta Biomater. **9**, 4457–4486 (2013). https://doi.org/10.1016/j.actbio.2012.08.023
9. T. Kokubo, H. Takadama, How useful is SBF in predicting in vivo bone bioactivity? Biomaterials **27**, 2907–2915 (2006). https://doi.org/10.1016/j.biomaterials.2006.01.017
10. International Organization for Standardization, *ISO—ISO 23317:2014—Implants for Surgery—In Vitro Evaluation for Apatite-Forming Ability of Implant Materials* (ISO). https://www.iso.org/standard/65054.html
11. A. Maçon, T. Kim, E. Valliant, K. Goetschius, R. Brow, D. Day, A. Hoppe, A. Boccaccini, I. Kim, C. Ohtsuki, T. Kokubo, A. Osaka, M. Vallet-Regí, D. Arcos, L. Fraile, A. Salinas, A. Teixeira, Y. Vueva, R. Almeida, M. Miola, C. Vitale-Brovarone, E. Verné, W. Höland, J. Jones, A unified in vitro evaluation for apatite-forming ability of bioactive glasses and their variants. J. Mater. Sci. Mater. Med. **26**, 1–10 (2015). https://doi.org/10.1007/s10856-015-5403-9
12. S. Yue, P.D. Lee, G. Poologasundarampillai, J.R. Jones, Evaluation of 3-D bioactive glass scaffolds dissolution in a perfusion flow system with X-ray microtomography. Acta Biomater. **7**, 2637–2643 (2011). https://doi.org/10.1016/j.actbio.2011.02.009
13. G. Theodorou, O.M. Goudouri, E. Kontonasaki, X. Chatzistavrou, L. Papadopoulou, N. Kantiranis, K.M. Paraskevopoulos, Comparative bioactivity study of 45S5 and 58S bioglasses in organic and inorganic environment. Bioceram. Dev. Appl. **1**, 1–4 (2011). https://doi.org/10.4303/bda/D110154
14. D. Rohanová, A.R. Boccaccini, D.M. Yunos, D. Horkavcová, I. Březovská, A. Helebrant, TRIS buffer in simulated body fluid distorts the assessment of glass–ceramic scaffold bioactivity. Acta Biomater. **7**, 2623–2630 (2011). https://doi.org/10.1016/j.actbio.2011.02.028
15. D. Zhang, M. Hupa, H.T. Aro, L. Hupa, Influence of fluid circulation on in vitro reactivity of bioactive glass particles. Mater. Chem. Phys. **111**, 497–502 (2008). https://doi.org/10.1016/j.matchemphys.2008.04.055
16. S. Fagerlund, P. Ek, L. Hupa, M. Hupa, Dissolution kinetics of a bioactive glass by continuous measurement. J. Am. Ceram. Soc. **95**, 3130–3137 (2012). https://doi.org/10.1111/j.1551-2916.2012.05374.x
17. R.E. Tomlinson, M.J. Silva, Skeletal blood flow in bone repair and maintenance. Bone Res. **1**, 311–322 (2013). https://doi.org/10.4248/BR201304002
18. M. Marenzana, T.R. Arnett, The key role of the blood supply to bone. Bone Res. **1**, 203–215 (2013). https://doi.org/10.4248/BR201303001
19. S. Salles, J. Shepherd, H.J. Vos, G. Renaud, Revealing intraosseous blood flow in the human tibia with ultrasound. JBMR Plus (2021). https://doi.org/10.1002/jbm4.10543
20. M. Laroche, Intraosseous circulation from physiology to disease. Jt Bone Spine **69**, 262–269 (2002). https://doi.org/10.1016/S1297-319X(02)00391-3
21. A. Stiller, M. Engblom, O. Karlström, M. Lindén, L. Hupa, Impact of fluid flow rate on the dissolution behavior of bioactive glass S53P4. J. Non-Cryst. Solids **607**, 122219 (2023). https://doi.org/10.1016/j.jnoncrysol.2023.122219
22. L. Bingel, D. Groh, N. Karpukhina, D.S. Brauer, Influence of dissolution medium pH on ion release and apatite formation of Bioglass 45S5. Mater. Lett. **143**, 279–282 (2015)
23. M. Cicuéndez, J.C. Doadrio, A. Hernández, M.T. Portolés, I. Izquierdo-Barba, M. Vallet-Regí, Multifunctional pH sensitive 3D scaffolds for treatment and prevention of bone infection. Acta Biomater. **65**, 450–461 (2018). https://doi.org/10.1016/j.actbio.2017.11.009
24. L. Drago, D. Romanò, E. De Vecchi, C. Vassena, N. Logoluso, R. Mattina, C.L. Romanò, Bioactive glass BAG-S53P4 for the adjunctive treatment of chronic osteomyelitis of the long bones: an in vitro and prospective clinical study. BMC Infect. Dis. **13**, 584 (2013). https://doi.org/10.1186/1471-2334-13-584
25. N.C. Lindfors, P. Hyvönen, M. Nyyssönen, M. Kirjavainen, J. Kankare, E. Gullichsen, J. Salo, Bioactive glass S53P4 as bone graft substitute in treatment of osteomyelitis. Bone **47**, 212–218 (2010). https://doi.org/10.1016/j.bone.2010.05.030
26. E. Steinhausen, R. Lefering, M. Glombitza, N. Brinkmann, C. Vogel, B. Mester, M. Dudda, Bioactive glass S53P4 vs. autologous bone graft for filling defects in patients with chronic osteomyelitis and infected non-unions—a single center experience. JBJI **6**, 73–83 (2021). https://doi.org/10.5194/jbji-6-73-2021
27. C.M. Agrawal, K.A. Athanasiou, Technique to control pH in vicinity of biodegrading PLA-PGA implants. J. Biomed. Mater. Res. **38**, 105–114 (1997). https://doi.org/10.1002/(SICI)1097-4636(199722)38:2%3c105::AID-JBM4%3e3.0.CO;2-U
28. H.E. Skallevold, D. Rokaya, Z. Khurshid, M.S. Zafar, Bioactive glass applications in dentistry. Int. J. Mol. Sci. **20**, 5960 (2019). https://doi.org/10.3390/ijms20235960
29. C. Loke, J. Lee, S. Sander, L. Mei, M. Farella, Factors affecting intra-oral pH—a review. J. Oral Rehabil. **43**, 778–785 (2016). https://doi.org/10.1111/joor.12429
30. G. Vergnol, N. Ginsac, P. Rivory, S. Meille, J.-M. Chenal, S. Balvay, J. Chevalier, D.J. Hartmann, In vitro and in vivo evaluation of a polylactic acid-bioactive glass composite for bone fixation devices. J. Biomed. Mater. Res. B **104**, 180–191 (2016). https://doi.org/10.1002/jbm.b.33364
31. M.A. Elsawy, K.-H. Kim, J.-W. Park, A. Deep, Hydrolytic degradation of polylactic acid (PLA) and its composites. Renew. Sustain. Energy Rev. **79**, 1346–1352 (2017). https://doi.org/10.1016/j.rser.2017.05.143
32. L. Björkvik, X. Wang, L. Hupa, Dissolution of bioactive glasses in acidic solutions with the focus on lactic acid. Int. J. Appl. Glass Sci. **7**, 154–163 (2016). https://doi.org/10.1111/ijag.12198
33. M. Arango-Ospina, L. Hupa, A.R. Boccaccini, Bioactivity and dissolution behavior of boron-containing bioactive glasses under static and dynamic conditions in different media. Biomed. Glass **5**, 124–139 (2019). https://doi.org/10.1515/bglass-2019-0011
34. M.M. Pereira, L.L. Hench, Mechanisms of hydroxyapatite formation on porous gel-silica substrates. J. Sol-Gel Sci. Technol. **7**, 59–68 (1996). https://doi.org/10.1007/BF00401884
35. M. Siekkinen, O. Karlström, L. Hupa, Effect of local ion concentrations on the in vitro reactions of bioactive glass 45S5 particles. Int. J. Appl. Glass Sci. **13**, 695–707 (2022). https://doi.org/10.1111/ijag.16579
36. M. Siekkinen, O. Karlström, L. Hupa, Dissolution of bioactive glass S53P4 in a three-reactor cascade in continuous flow conditions. Open Ceram. **13**, 100327 (2023). https://doi.org/10.1016/j.oceram.2022.100327
37. I.D. Xynos, A.J. Edgar, L.D.K. Buttery, L.L. Hench, J.M. Polak, Ionic products of bioactive glass dissolution increase proliferation of human osteoblasts and induce insulin-like growth factor II mRNA expression and protein synthesis. Biochem. Biophys. Res. Commun. **276**, 461–465 (2000). https://doi.org/10.1006/bbrc.2000.3503
38. K. Vuornos, M. Ojansivu, J.T. Koivisto, H. Häkkänen, B. Belay, T. Montonen, H. Huhtala, M. Kääriäinen, L. Hupa, M. Kellomäki, J. Hyttinen, J.A. Ihalainen, S. Miettinen, Bioactive glass ions induce efficient osteogenic differentiation of human adipose stem cells

encapsulated in gellan gum and collagen type I hydrogels. Mater. Sci. Eng. C **99**, 905–918 (2019). https://doi.org/10.1016/j.msec.2019.02.035
39. M. Ojansivu, S. Vanhatupa, L. Björkvik, H. Häkkänen, M. Kellomäki, R. Autio, J.A. Ihalainen, L. Hupa, S. Miettinen, Bioactive glass ions as strong enhancers of osteogenic differentiation in human adipose stem cells. Acta Biomater. **21**, 190–203 (2015). https://doi.org/10.1016/j.actbio.2015.04.017
40. M. Siekkinen, M. Engblom, L. Hupa, Impact of solution pH (5–9) and dissolution products on in vitro behaviour of the bioactive glass S53P4. J. Non-Cryst. Solids X **20**, 100199 (2023). https://doi.org/10.1016/j.nocx.2023.100199
41. V. Aina, L. Bertinetti, G. Cerrato, M. Cerruti, G. Lusvardi, G. Malavasi, C. Morterra, L. Tacconi, L. Menabue, On the dissolution/reaction of small-grain Bioglass® 45S5 and F-modified bioactive glasses in artificial saliva (AS). Appl. Surf. Sci. **257**, 4185–4195 (2011). https://doi.org/10.1016/j.apsusc.2010.12.019
42. M. Cerruti, D. Greenspan, K. Powers, Effect of pH and ionic strength on the reactivity of Bioglass® 45S5. Biomaterials **26**, 1665–1674 (2005). https://doi.org/10.1016/j.biomaterials.2004.07.009
43. N. Stone-Weiss, R.E. Youngman, R. Thorpe, N.J. Smith, E.M. Pierce, A. Goel, An insight into the corrosion of alkali aluminoborosilicate glasses in acidic environments. Phys. Chem. Chem. Phys. **22**, 1881–1896 (2020). https://doi.org/10.1039/C9CP06064B
44. Q. Qin, N. Stone-Weiss, T. Zhao, P. Mukherjee, J. Ren, J.C. Mauro, A. Goel, Insights into the mechanism and kinetics of dissolution of aluminoborosilicate glasses in acidic media: impact of high ionic field strength cations. Acta Mater. **242**, 118468 (2023). https://doi.org/10.1016/j.actamat.2022.118468
45. E. Fernández, F.J. Gil, M.P. Ginebra, F.C.M. Driessens, J.A. Planell, S.M. Best, Calcium phosphate bone cements for clinical applications. Part I: solution chemistry. J. Mater. Sci. Mater. Med. **10**, 169–176 (1999). https://doi.org/10.1023/A:1008937507714
46. S.V. Dorozhkin, Calcium orthophosphates ($CaPO_4$): occurrence and properties. Prog. Biomater. **5**, 9–70 (2016). https://doi.org/10.1007/s40204-015-0045-z
47. J.G. Neves, D. Navarro da Rocha, C.C. Lopes, M.H. Prado da Silva, M.A.C. Sinhoreti, L. Correr-Sobrinho, M.A.A. Fraga, A.B. Correr, Effect of pH level and calcination on the production of calcium phosphates by acidic route of wet precipitation. Cerâmica **67**, 236–243 (2021). https://doi.org/10.1590/0366-69132021673822965
48. R.K. Iler, The solubility of silica. In: *The Chemistry of Silica* (Wiley, Hoboken, 1979), pp. 30–49
49. R.W. Douglas, T.M.M. El-Shamy, Reactions of glasses with aqueous solutions. J. Am. Ceram. Soc. **50**, 1–8 (1967). https://doi.org/10.1111/j.1151-2916.1967.tb14960.x
50. M. Höner, F. Böke, M. Weber, H. Fischer, Mimicking physiological flow conditions to study alterations of bioactive glass surfaces in vitro: MIMICKING PHYSIOLOGICAL FLOW CONDITIONS. J. Biomed. Mater. Res. **106**, 228–236 (2018). https://doi.org/10.1002/jbm.b.33847
51. M. Par, A. Gubler, T. Attin, Z. Tarle, A. Tarle, T.T. Tauböck, Ion release and hydroxyapatite precipitation of resin composites functionalized with two types of bioactive glass. J. Dent. **118**, 103950 (2022). https://doi.org/10.1016/j.jdent.2022.103950
52. P. Sinitsyna, O. Karlström, L. Hupa, In vitro dissolution of bioactive glass S53P4 microspheres. J. Am. Ceram. Soc. **105**, 1658–1670 (2022). https://doi.org/10.1111/jace.18014
53. P. Sinitsyna, O. Karlström, C. Sevonius, L. Hupa, In vitro dissolution and characterisation of flame-sprayed bioactive glass microspheres S53P4 and 13–93. J. Non-Cryst. Solids **591**, 121736 (2022). https://doi.org/10.1016/j.jnoncrysol.2022.121736
54. L. Aalto-Setälä, M. Siekkinen, N. Lindfors, L. Hupa, Dissolution of glass–ceramic scaffolds of bioactive glasses 45S5 and S53P4. Biomed. Mater. Devices (2023). https://doi.org/10.1007/s44174-022-00059-4
55. I. Izquierdo-Barba, A.J. Salinas, M. Vallet-Regí, Effect of the continuous solution exchange on the in vitro reactivity of a CaO–SiO_2 sol–gel glass. J. Biomed. Mater. Res. **51**, 191–199 (2000). https://doi.org/10.1002/(SICI)1097-4636(200008)51:2%3c191::AID-JBM7%3e3.0.CO;2-T
56. D. Galusková, H. Kaňková, A. Švančárková, D. Galusek, Early-stage dissolution kinetics of silicate-based bioactive glass under dynamic conditions: critical evaluation. Materials **14**, 3384 (2021). https://doi.org/10.3390/ma14123384
57. E. Eriksson, R. Björkenheim, G. Strömberg, M. Ainola, P. Uppstu, L. Aalto-Setälä, V.-M. Leino, L. Hupa, J. Pajarinen, N.C. Lindfors, S53P4 bioactive glass scaffolds induce BMP expression and integrative bone formation in a critical-sized diaphysis defect treated with a single-staged induced membrane technique. Acta Biomater. **126**, 463–476 (2021). https://doi.org/10.1016/j.actbio.2021.03.035